Electronic Supplementary Material (ESI) for Chemical Communications.
This journal is © The Royal Society of Chemistry 2020

Electronic Supplementary Information (ESI)

Thermo-and electro switchable Cs$\subset$\{Fe_4Fe_4\} cubic cage: Spin-Transition and Electrochromism

Jana Glatz,[a] Lise-Marie Chamoreau,[a] Alexandrine Flambard,[a] Jean-Francois Meunier,[b] Azzedine Bouseksou[b] and Rodrigue Lescouëzec*[a]

[a]Sorbonne Université, CNRS, Institut Parisien de Chimie Moléculaire, F-75005 Paris France, e-mail : rodrigue.lescouezec@sorbonne-universite.fr

Section S1 - Experimental and technical details

Section S1.1 Synthetic procedure

To a yellow solution of the $NBu_4[Fe^{III}(Tp)CN]$ (293mg, 0.5 mmol) dissolved in 3 mL of DMF, is added the salt $Fe^{II}(ClO_4)_2 \bullet H_2O$ (140 mg, 0.5 mmol) as a solid. The solution immediately turns dark green indicating the formation of $(Tp)Fe^{II}$-CN-Fe^{III} linkages. Then a solution of a $CsClO_4$ salt in 3mL DMF is added drop wise and the dark green solution is stirred for five minutes before adding the blocking ligand Na(pzTp) as a solid (150 mg, 0.5 mmol). A colour change from dark green to murky grass green can be observed at that stage. The solution is stirred overnight forming a dark green precipitate, which is separated from the solution by centrifuging. In order to get rid of the unwanted $\{Fe^{II}(pzTp)_2\}$ sandwich complex that forms, the obtained solid is washed with a mixture of DMF/Et_2O (1:8) till the filtrate is no longer light pink but transparent or light green. The product can then be crystalized in pure acetonitrile. Yield: (60 %).

^{133}Cs NMR (CD_2Cl_2, 300 K) ∂ = 925 ppm, Elemental Analysis (C, H, N) : $CsC_{96}H_{88}B_8Fe_8N_{68} \cdot 0.6\ CH_3CN \cdot 2\ H_2O$ calculated (found): 41.29 (41.31),3.35 (3.32), 33.96 (33.96).

Note: ClO_4^- salts are explosive and should be handled with care, avoiding grinding, using glass spatula and working at room temperature (none of the solution was heating).

Section S1.2 Technical Details

FT-IR spectra were collected in the 400 - 4000 cm^{-1} range. Measurements were carried out on solid samples in ATR mode on a Vertex 70 Bruker instrument (4 cm^{-1} resolution).

Mass spectrometric analyses (ESI mode) were performed on a quadrupole Orbitrap Q Exactive mass spectrometer from Thermo Scientific.

X-Ray crystallography. A single crystal of the compound was selected, mounted onto a cryoloop, and transferred in the cold nitrogen gas stream of an Oxford Cryostream. Intensity data were collected with a BRUKER Kappa-APEXII diffractometer with micro-focused Cu-Kα radiation at 200K. APEX 3 suite and SAINT program (BRUKER) were used to carry out data collection, unit-cell parameters refinement, integration and data reduction. SADABS (BRUKER) was used for scaling and multi-scan absorption corrections. Due to the very small size of the sample and the low scattering power of the sample, the data were collected only up to 1.0 Å. In the Olex2 suite[1], the structure was solved with SHELXT-14 program[2] and refined by full-matrix least-squares methods using SHELXL-14.[3]

From this dataset, we refined the crystal structure model with two different approaches :

1. Signal over noise ratio above 1.15 Å was largely under 3 and dataset was thus truncated at this latter value of resolution. The low resolution of the dataset (and thus low number of data) prevented the anisotropic refinement of atoms other than caesium and iron ones. A large number of solvent molecules are present in the structure. The ones closest to the Fe8 cages were located on the Fourier difference maps but for the further ones we used a SQUEEZE procedure because the remaining electronic density was too diffuse. Several restrains and constraints were introduced for solvent molecules.

   This approach allows to get some structural features about supramolecular assembling of cubic cages and the interaction of the latter with ACN or DMF molecules. (CCDC 2009994)
2. On the other hand, in order to improve the quality of the structural model of the Fe8 cage, we used a SQUEEZE procedure for the whole solvent sphere. This allows an anisotropic refinement of all the atoms of the cages. (CCDC 2020986)

CCDC 2009994 and 2020986 contain the supplementary crystallographic data for this paper. The data can be obtained free of charge from The Cambridge Crystallographic Data Centre via www.ccdc.cam.ac.uk/structures.

Elemental Analysis (C, H, N) were carried out by combustion analysis using vario MICRO cube apparatus from Elementar.

DC Magnetic susceptibility measurements were performed in a Quantum Design SQUID magnetometer. The sample (packed in a polyethylene bag) was introduced under helium flow at 110 K to avoid solvent evaporation. All data were corrected by estimating the diamagnetic contribution of the sample and sample holder.

---

[1] O. V. Dolomanov, L. J. Bourhis, R. J. Gildea, J. A. K. Howard, H. Puschmann, *J. Appl. Cryst.* **2009**, *42*, 339–341..

[2] G. M. Sheldrick, *Acta Crystallographica Section A* **2015**, *71*, 3–8..

[3] G. M. Sheldrick, *Acta Crystallographica Section C* **2015**, *71*, 3–8.

Cyclic voltammetry measurements were carried out at 18 °C under nitrogen atmosphere in a standard cell equipped with a platinum wire counter electrode, a calomel reference electrode (SCE) and a glassy carbon working electrode (3 mm) using an AUTOLAB PGSTAT 100 electrochemical analyzer. Measurements were performed in CH_2Cl_2 and CH_3CN solution with 0.1 M $[NBu_4][PF_6]$ as supporting electrolyte at scan rates between 50-100 mVs^{-1}.

UV-vis-NIR absorption spectra were measured in the range between 200-2000 nm in a CARY 4000 UV-vis spectrophotometer.

Spectro-electrochemical measurements were performed in an optically transparent thin-layer electrochemical cell (OTTLE from Reading University), which is specifically designed to be inserted in standard UV-vis spectrometer. The cell contains a platinum counter electrode and a platinum mesh working electrode. Measurements were performed in CH_3CN solution with 0.1 M $[NBu_4][PF_6]$ as supporting electrolyte at scan rate of 100 mVs^{-1}.

^{57}Fe Mössbauer spectroscopy of freshly filtered crystals (50 mg) were recorded using a conventional constant-acceleration-type spectrometer equipped with a 50 mCi ^{57}Co source and a liquid-N_2 cryostat. The spectra were recorded at 80 K under reduced helium pressure and 300 K. Least-square fittings of the Mössbauer spectra were performed considering line shapes using the Recoil software package.

Thermogravimetric Analysis (TGA) was carried out with a TGA analyser (TAI instrument, SDT Q600) at a rate of 2 °C min^{-1} under a dinitrogen flow (100mL/min).

Section S2 Crystallographic details

Table S1. Crystal data and structure refinement of $Cs\subset\{Fe_4\text{-}Fe_4\}$ cube with *approach 1*

Empirical formula	$C_{135.13}H_{166.5}B_8CsFe_8N_{84.63}O_{8.38}$
Formula weight	3776.46
Temperature/K	200
Crystal system	triclinic
Space group	P-1
a/Å	22.9028(8)
b/Å	25.6517(10)
c/Å	37.4088(16)
α/°	103.765(2)
β/°	103.906(2)
γ/°	90.208(2)
Volume/Å^3	20677.5(14)
Z	4
ρ_{calc}g/cm^3	1.213
μ/mm^{-1}	6.263
F(000)	7758.0
Crystal size/mm^3	0.12 × 0.1 × 0.06
Radiation	CuKα (λ = 1.54178)
2Θ range for data collection/°	3.814 to 84.186
Index ranges	$-19 \leq h \leq 19$, $-22 \leq k \leq 21$, $-32 \leq l \leq 32$
Reflections collected	81787
Independent reflections	28249 [R_{int} = 0.1038, R_{sigma} = 0.1012]
Data/restraints/parameters	28249/44/2120
Goodness-of-fit on F^2	1.038
Final R indexes [I>=2σ (I)]	R_1 = 0.1265, wR_2 = 0.3036
Final R indexes [all data]	R_1 = 0.1731, wR_2 = 0.3374
Largest diff. peak/hole / e Å^{-3}	2.15/-1.76
CCDC deposition number	2009994

Table S2 : Crystal data and structure refinement for $Cs\subset\{Fe_4\text{-}Fe_4\}$ cube with *approach 2*.

Empirical formula	$C_{184}H_{262.5}B_8CsFe_8N_{103.5}O_{17}$
Formula weight	4862.65
Temperature/K	200
Crystal system	triclinic
Space group	P-1
a/Å	22.9028(8)
b/Å	25.6517(10)
c/Å	37.4088(16)
α/°	103.765(2)
β/°	103.906(2)
γ/°	90.208(2)
Volume/Å3	20677.5(14)
Z	4
ρcalcg/cm3	1.562
μ/mm-1	6.463
F(000)	10120.0
Crystal size/mm3	0.12 × 0.1 × 0.06
Radiation	CuKα (λ = 1.54178)
2Θ range for data collection/°	3.554 to 88.982
Index ranges	-20 ≤ h ≤ 20, -23 ≤ k ≤ 22, -34 ≤ l ≤ 33
Reflections collected	90692
Independent reflections	32321 [Rint = 0.1108, Rsigma = 0.1122]
Data/restraints/parameters	32321/4830/3259
Goodness-of-fit on F2	1.029
Final R indexes [I>=2σ (I)]	R1 = 0.1047, wR2 = 0.2530
Final R indexes [all data]	R1 = 0.1496, wR2 = 0.2832
Largest diff. peak/hole / e Å-3	2.08/-1.78
CCDC reference number	2020986

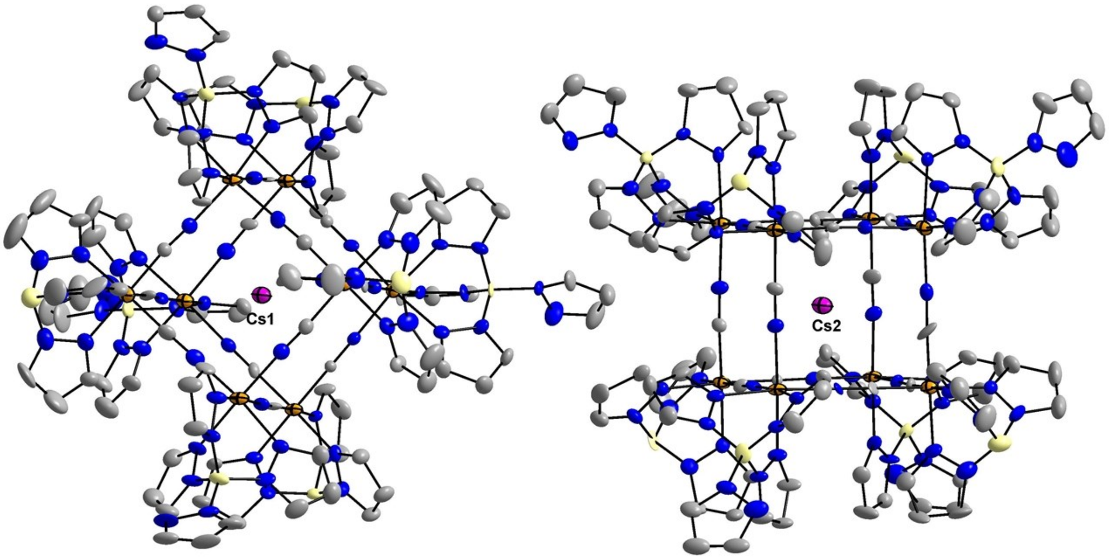

Figure S1. Asymetric unit (containing two independent cubic molecules) of the crystal structure with displacement parameters at 30% (H atoms and solvent molecules were omitted for clarity)

Table S3. Distances between caesium and iron atoms.

In molecule 1		(in Å)
Cs1	Fe2	4.203
Cs1	Fe6	4.341
Cs1	Fe8	4.365
Cs1	Fe4	4.376
Cs1	Fe3	4.422
Cs1	Fe1	4.434
Cs1	Fe7	4.484
Cs1	Fe5	4.555
In molecule 2		
Cs2	Fe12	4.201
Cs2	Fe16	4.361
Cs2	Fe14	4.362
Cs2	Fe10	4.378
Cs2	Fe13	4.425
Cs2	Fe11	4.451
Cs2	Fe9	4.488
Cs2	Fe15	4.516

Table S4. Selected bond lengths in the two crystallographically independent cubic molecules *from approach 2*

Atom	Atom	Length/Å	Atom	Atom	Length/Å
Fe1	C1	1.85(2)	Fe9	C13	1.852(19)
Fe1	C2	1.797(19)	Fe9	C14	1.893(19)
Fe1	C3	1.89(2)	Fe9	C15	1.79(2)
Fe1	N3A	2.055(17)	Fe9	N1I	2.034(15)
Fe1	N5A	1.985(17)	Fe9	N3I	2.013(14)
Fe1	N1AA	2.024(16)	Fe9	N5I	2.028(14)
Fe2	N1	2.007(18)	Fe10	N13	2.016(15)
Fe2	N4	2.060(15)	Fe10	N16	1.996(14)
Fe2	N10	2.048(18)	Fe10	N22	2.012(16)
Fe2	N1B	2.071(14)	Fe10	N1J	2.128(13)
Fe2	N3B	2.103(15)	Fe10	N3J	2.155(15)
Fe2	N5B	2.137(15)	Fe10	N5J	2.113(14)
Fe3	C4	1.908(19)	Fe11	C16	1.859(18)
Fe3	C5	1.85(2)	Fe11	C17	1.95(2)
Fe3	C6	1.836(19)	Fe11	C18	1.844(19)
Fe3	N1C	2.026(15)	Fe11	N1K	1.994(14)
Fe3	N3C	2.008(12)	Fe11	N3K	1.985(14)
Fe3	N5C	1.994(14)	Fe11	N5K	2.000(14)
Fe4	N2	2.045(15)	Fe12	N14	2.047(15)
Fe4	N5	2.046(16)	Fe12	N17	2.058(16)
Fe4	N7	2.085(18)	Fe12	N19	2.041(15)
Fe4	N1D	2.138(16)	Fe12	N1L	2.119(15)
Fe4	N3D	2.132(16)	Fe12	N3L	2.087(13)
Fe4	N5D	2.143(15)	Fe12	N5L	2.133(15)
Fe5	C7	1.86(2)	Fe13	C19	1.875(19)
Fe5	C8	1.816(19)	Fe13	C20	1.92(2)
Fe5	C9	1.880(19)	Fe13	C21	1.913(18)
Fe5	N1E	1.984(13)	Fe13	N1M	2.013(14)
Fe5	N3E	1.975(15)	Fe13	N3M	2.000(13)
Fe5	N5E	2.020(16)	Fe13	N5M	2.013(13)
Fe6	N3	2.048(16)	Fe14	N15	2.051(16)
Fe6	N8	2.006(15)	Fe14	N20	2.034(16)
Fe6	N11	2.006(16)	Fe14	N23	2.047(15)
Fe6	N1F	2.132(15)	Fe14	N1N	2.192(14)
Fe6	N3F	2.120(13)	Fe14	N3N	2.123(15)
Fe6	N5F	2.171(15)	Fe14	N5N	2.110(16)
Fe7	C10	1.89(2)	Fe15	C22	1.86(2)
Fe7	C11	1.87(2)	Fe15	C23	1.924(18)
Fe7	C12	1.835(19)	Fe15	C24	1.899(19)
Fe7	N1G	1.977(17)	Fe15	N1O	2.013(14)
Fe7	N3G	2.010(16)	Fe15	N3O	2.004(14)
Fe7	N5G	2.029(15)	Fe15	N5O	1.994(14)
Fe8	N6	2.035(15)	Fe16	N18	2.058(15)

Fe8	N9	2.056(15)	Fe16	N21	2.024(14)
Fe8	N12	2.026(14)	Fe16	N24	2.070(15)
Fe8	N1H	2.188(14)	Fe16	N1P	2.116(14)
Fe8	N3H	2.116(15)	Fe16	N3P	2.081(14)
Fe8	N5H	2.084(15)	Fe16	N5P	2.192(14)

Section S3 FT-IR spectroscopy

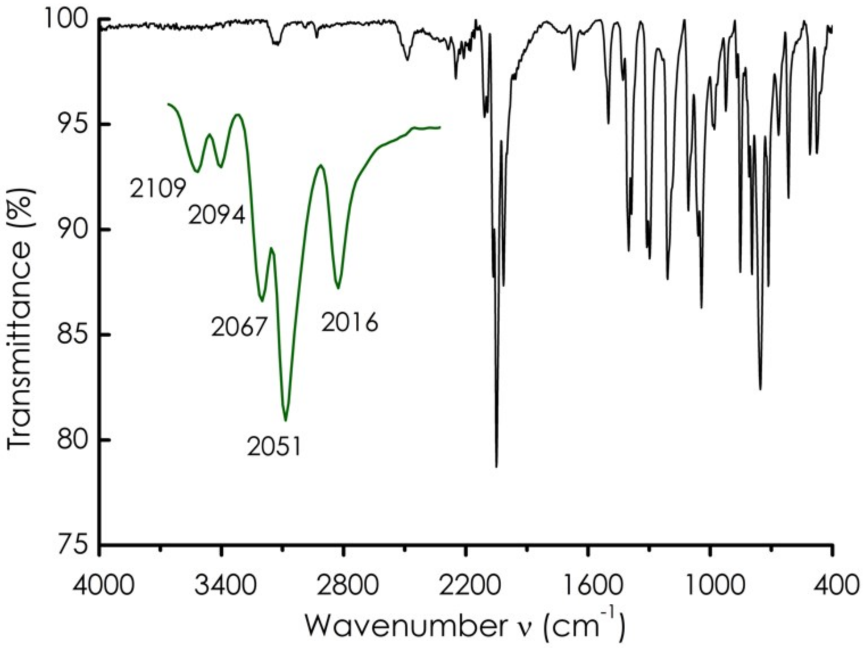

Figure S2. FT-IR (ATR) transmission spectra of fresh crystals of Cs⊂{Fe_4Fe_4}. Zoom of the FR-IR spectrum shows the cyanide stretching vibrations.

IR (ATR, ν in cm^{-1}): 349 (w), 375 (w), 405 (vw), 477 (w), 511 (w), 617 (w), 658 (w), 715 (m), 755 (m), 795 (m), 810 (w), 852 (w), 869 (vw), 924 (vw), 983 (w), 1045(w), 1059 (w), 1110 (w),1210 (br, w), 1297 (w), 1311(w), 1385 (m), 1403 (m), 1427 (w), 1501 (w), 1670(br, vw), 2016 (CN, w), 2051 (CN, m), 2067 (CN, w), 2094 (CN, vw), 2109 (CN, vw), 2485 (B-H, br, vw), 3129 (br, vw)

Section S4 Mass spectrometry

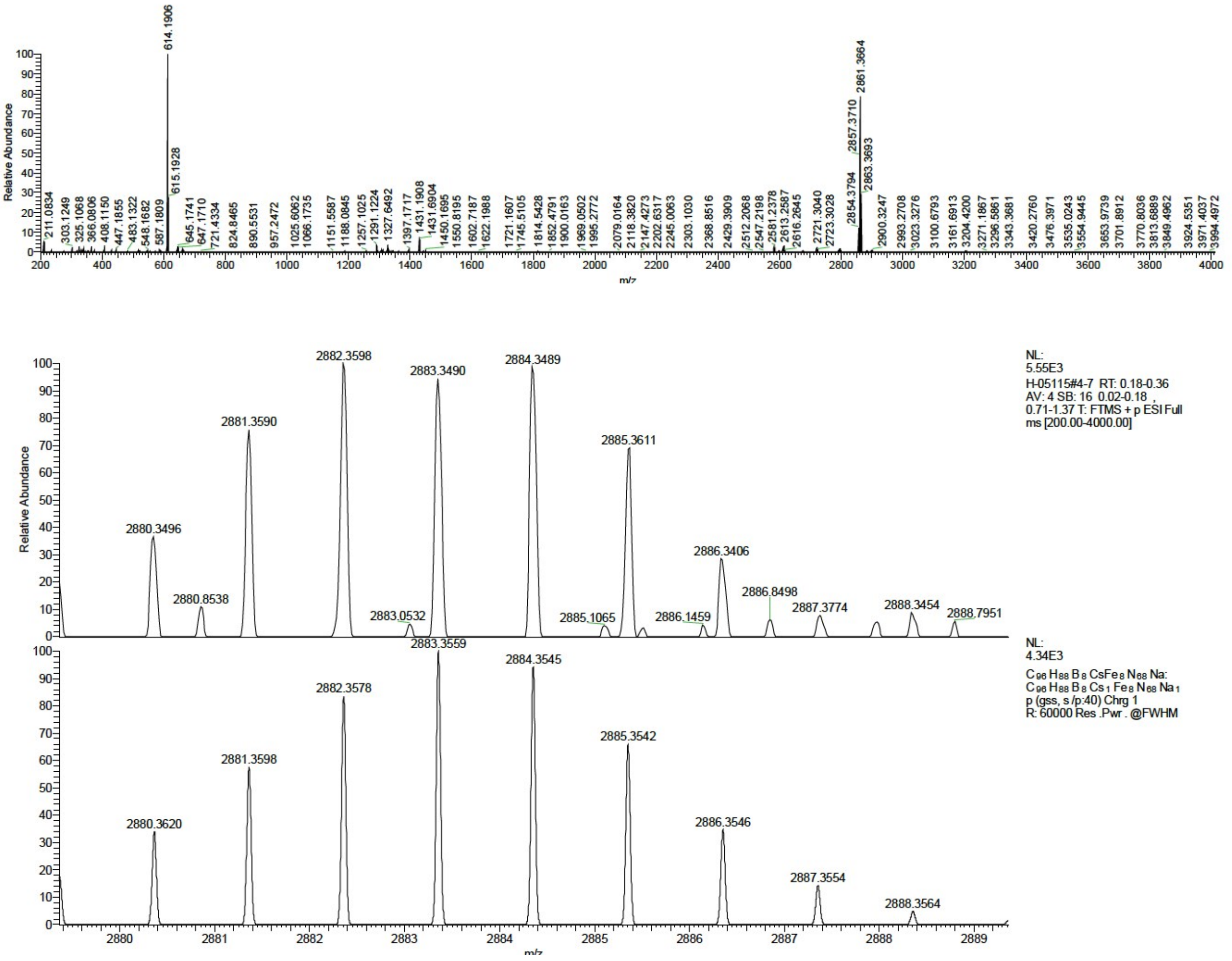

Figure S3. High Resolution ESI-mass spectrum of Cs⊂{Fe_4Fe_4} in CH_3CN.

Section S5 NMR

Section 5.1 ^1H NMR

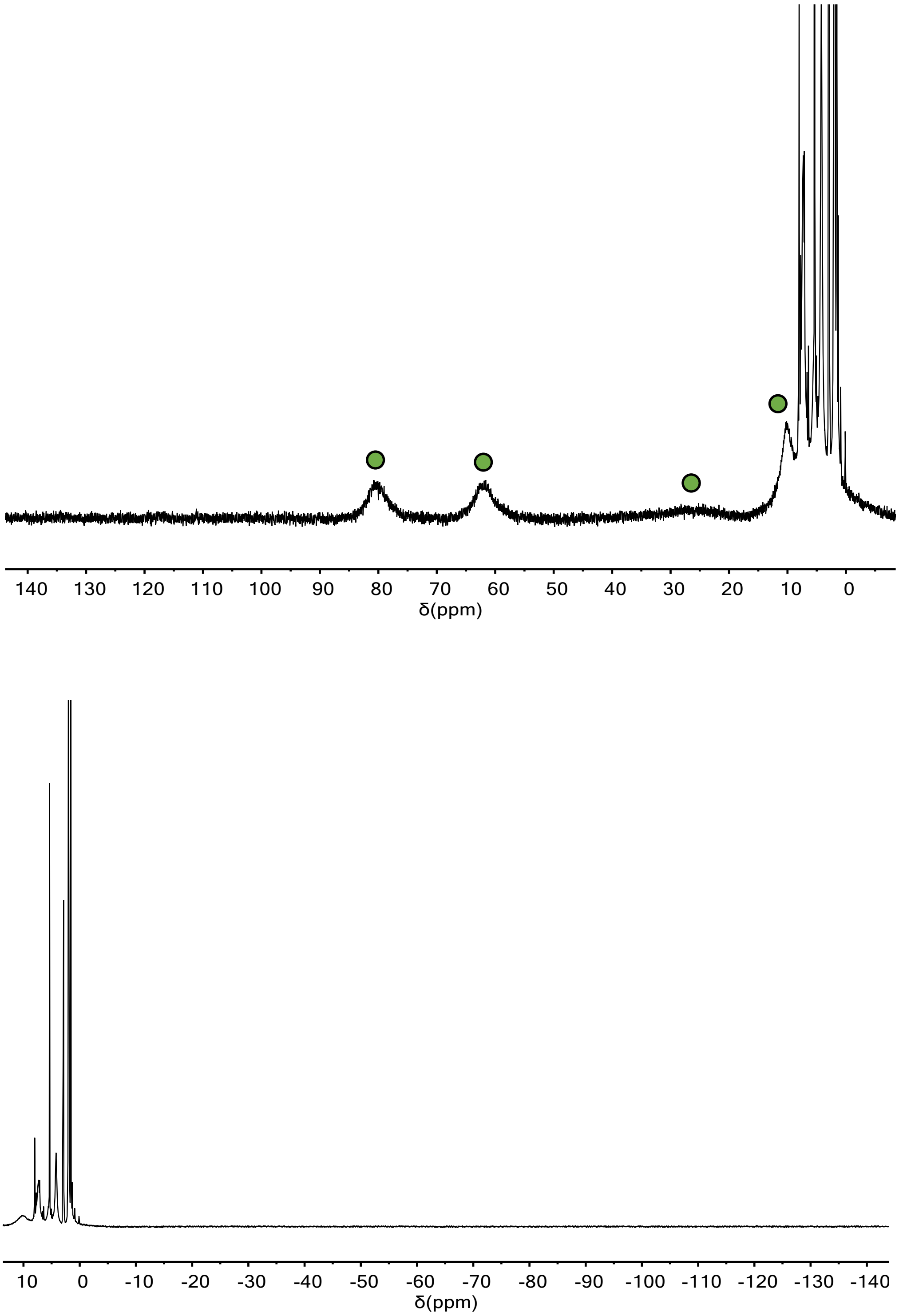

Figure S4. ^1H NMR of Cs⊂{Fe_4Fe_4} recorded at 300 K in CD_2Cl_2 solution (5 mM) in a 400 MHz spectrometer. The green dots depict signals that can be surely attributed to Cs⊂{Fe_4Fe_4}.

Section 5.2 ^{133}Cs

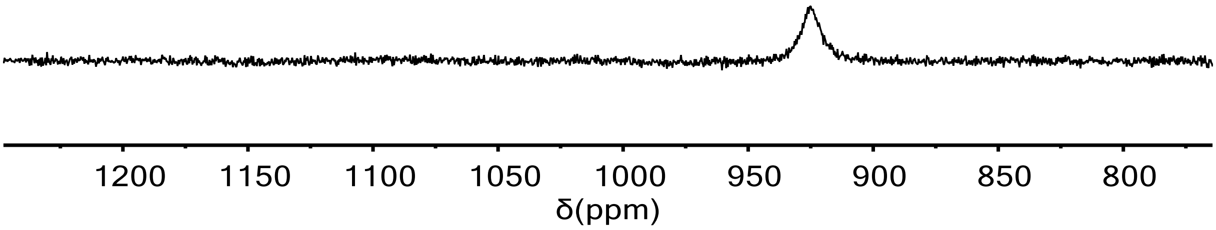

Figure S5. ^{133}Cs NMR of Cs⊂{Fe_4Fe_4} recorded at 300 K in CD_2Cl_2 solution (5 mM) in a 400 MHz spectrometer.

Section S6 Cyclic voltammetry studies

Section S6.1 CH_2Cl_2

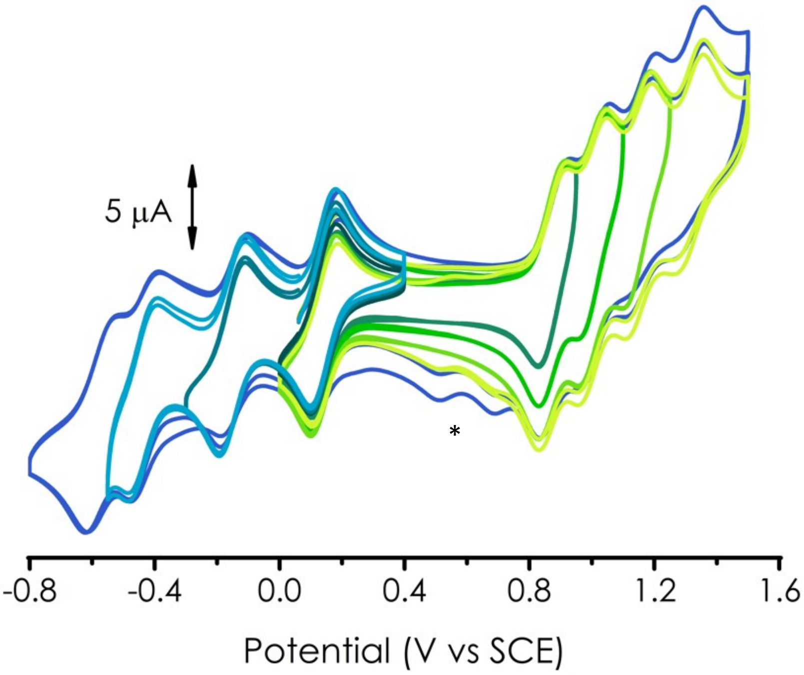

Figure S6. Cyclic voltammograms of Cs⊂{Fe_4Fe_4} in CH_2Cl_2 with 0.1 M Bu_4NPF_6 (potential vs. SCE, 0.33 mM, glassy carbon working electrode, Pt wire counter electrode; 100 mVs^{-1}). OCP around 0.05 V.

Section S6.2 Diffusion coefficient

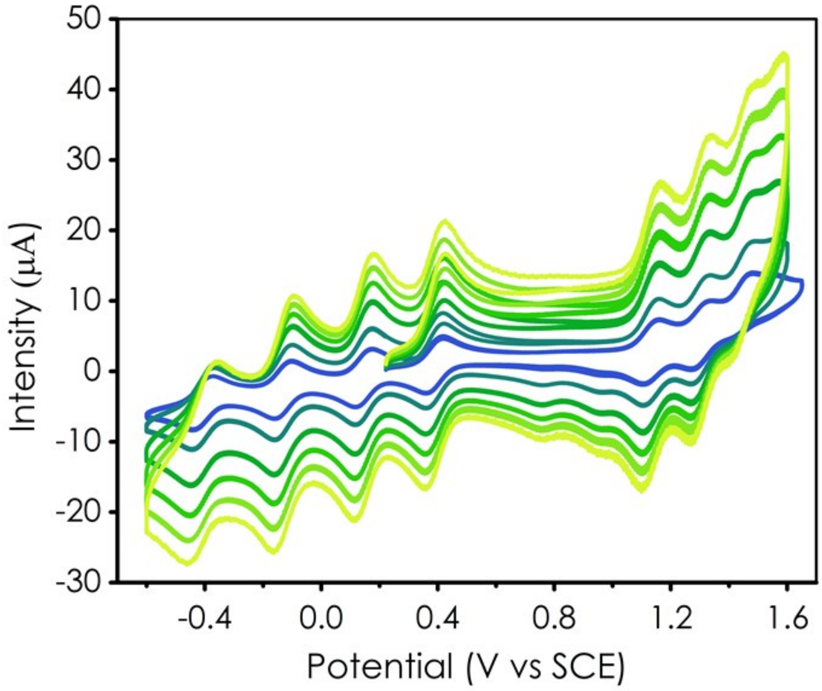

Figure S7. Cyclic voltammograms of Cs⊂{Fe_4Fe_4} in CH_3CN with 0.1 M Bu_4NPF_6 (potential vs. SCE 0.33 mM, glassy carbon working electrode, Pt wire counter electrode) taken at scan rates of 50, 100, 200, 300, 400, 500 mV s^{-1} (blue to yellow curves) at 18 °C. Open Circuit Potential at 0.2V.

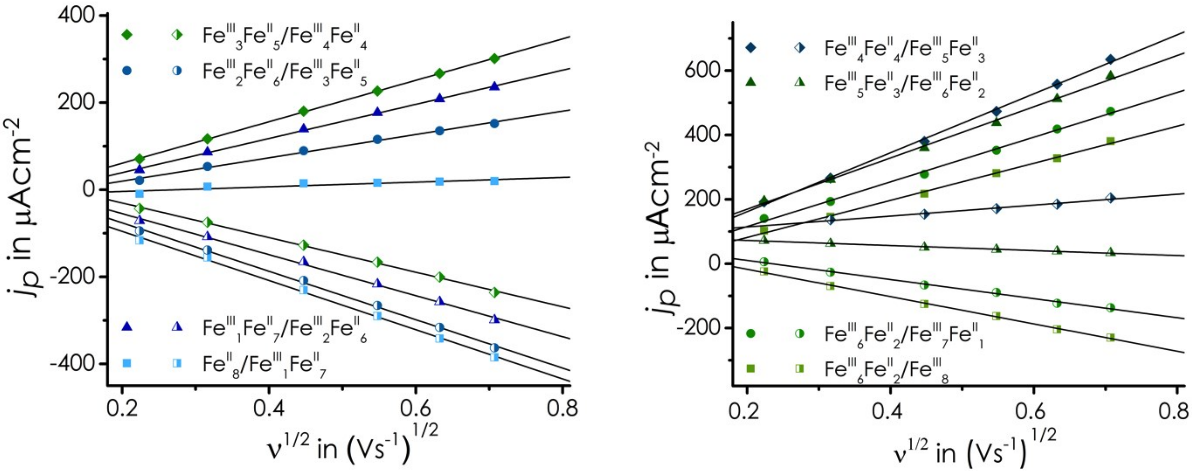

Figure S8. Linear Fit of the plot of the current density (j_p) versus the square root of the scan rate ($\nu^{1/2}$) extracted from the data in Fig S6.2.1

Randles-Sevcik equation:

$$j_p = 0.4436\ n_e F c_0 \left(\frac{nFD_0 v}{RT}\right)^{1/2}$$

$j_p =$ normalized current density A cm^2

$n_e =$ number of electrons transferred in the redox process

F = Faraday constant in C mol^{-1}

$D_0 =$ diffusion coefficient in cm^2 s^{-1}

$c_0 =$ bulk concentration of the species in solution in mol dm^{-3}

$v =$ voltage scan rate in V s^{-1}

R = Gas constant in J K^{-1} mol^{-1}

	m (10^{-6}(cm^2s^{-1})$^{1/2}$*mol* L^{-1})	D_0 (10^{-6} cm^2s^{-1})
$j_{p,a}^{1}$	-564.83864	39.21
$j_{p,a}^{2}$	-555.69084	37.95
$j_{p,a}^{3}$	-470.9841	27.26
$j_{p,a}^{4}$	-397.32104	19.40
$j_{p,c}^{1}$	53.65584	0.352
$j_{p,c}^{2}$	267.70985	8.81
$j_{p,c}^{3}$	392.01754	18.89
$j_{p,c}^{4}$	476.08635	27.86
$j_{p,a}^{5}$	-424.22341	22.12
$j_{p,a}^{6}$	-296.73486	10.82
$j_{p,a}^{7}$	-78.20321	0.75
$j_{p,a}^{8}$	169.86725	3.55
$j_{p,c}^{5}$	575.96651	40.77
$j_{p,c}^{6}$	694.3328	59.25
$j_{p,c}^{7}$	795.58449	77.79
$j_{p,c}^{8}$	915.87791	103.10

Table S4. Diffusion coefficients D_0 of Cs⊂{Fe_4Fe_4} calculated with the Randles-Revcik equation by using the slope *m* of the fitted straight lines (Figure S6.2.2)

Section S7 UV-vis-spectra and additional information for spectro-electrochemical analysis

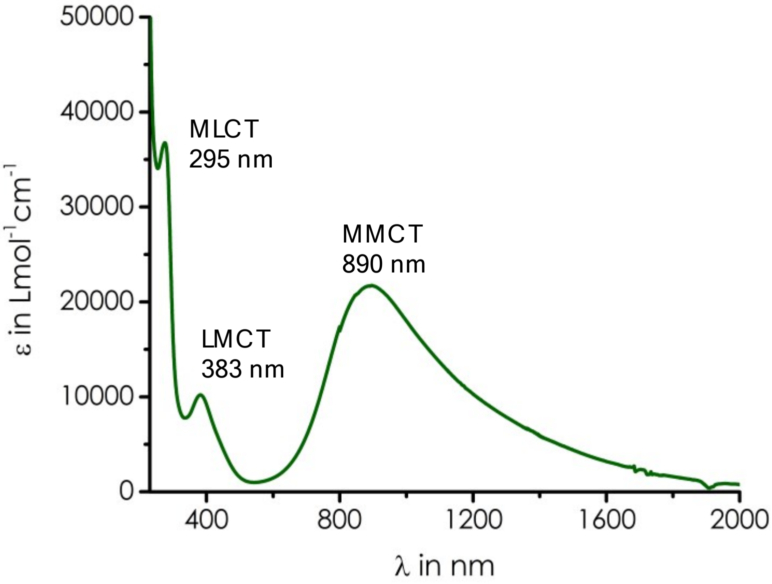

Figure S9. UV-Vis spectrum of Cs⊂{Fe_4Fe_4} in a CH_3CN solution at 0.05 mM.

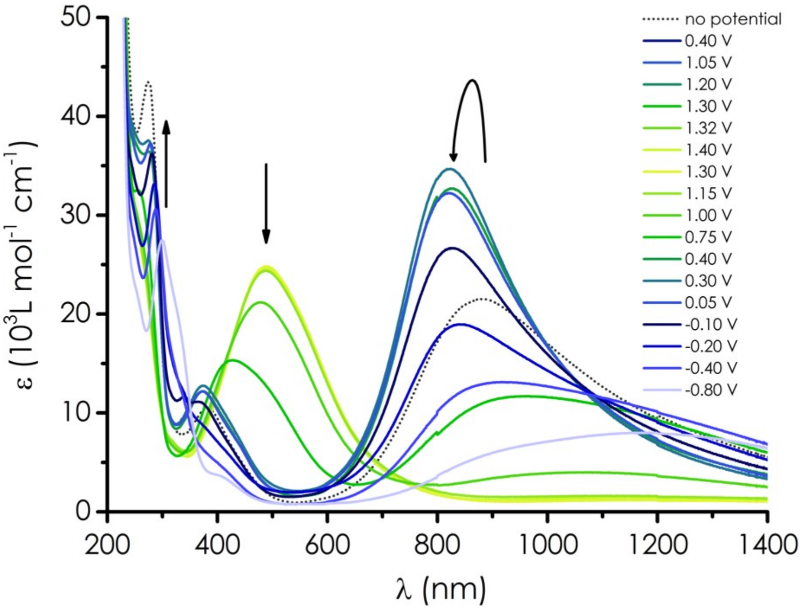

Figure S10. UV-vis spectra of Cs$\subset$\{Fe$_4$Fe$_4$\} in a CH$_3$CN solution at 0.5 mM at controlled potentials in the full range: -0.80 V — +1.40 V (vs SCE).

Additional details on attribution of the LMCT and MLCT bands.

The band around *ca.* 250-300 nm is associated with the overlapping MLCT bands of the \{Fe^{II}(Tp)($\underline{\mathrm{C}}$N)$_3$\} and \{Fe^{II}(pzTp)($\underline{\mathrm{N}}$C)$_3$\} sites. In fact, at high potential, in the \{Fe$^{III}_{4}$-Fe$^{III}_{4}$\} state, this band is not present. It only appears upon reduction, first around 270 nm. This first band is thus likely due to the MLCT of the \{Fe^{III}(Tp)(CN)$_3$\} units that get reduced (before the \{Fe^{III}(pzTp)($\underline{\mathrm{N}}$C)$_3$\} units) as the potential decreases from 1.6 V to 1 V (see CV experiment). At lower potential, upon further reduction a shoulder appears around 300 nm and it is attributed to the MLCT of the \{Fe^{II}(pzTp)(NC)$_3$\} moieties.

Similarly, the band between *ca* 350-500 nm observed at high potential, in the \{Fe$^{III}_{4}$-Fe$^{III}_{4}$\} state, is associated with the overlapping LMCT bands of the \{Fe^{III}(Tp)(CN)$_3$\} and \{Fe^{III}(pzTp)(NC)$_3$\} sites. This band slowly fades and shifts to lower wavelengths. This is probably due to the change of a mixed LMCT band containing the contribution of both Fe^{III} sites to the pure LMCT band of the \{Fe^{III}(pzTp)(NC)$_3$\}. This band almost disappear at very low potential (ca. -0.8 V) as the main species in solution is the Cs$\subset$\{Fe$^{II}_{4}$-Fe$^{II}_{4}$\} cube.

Around 0.4 V the cube is in the \{Fe$^{II}_{4}$-Fe$^{III}_{4}$\} state and shows a quite symmetrical band centered at 820 nm. Upon oxidation and reduction this band shifts to higher wavelengths and looses intensity. Simultaneously, upon reduction and oxidation, in each case there is a new band appearing which is centered around 1100 nm. These bands disappear once the cube either reached its oxidized \{Fe$^{III}_{4}$-Fe$^{III}_{4}$\} or reduced \{Fe$^{II}_{4}$-Fe$^{II}_{4}$\} state. These bands are tentatively associated with an electron transfer of remote iron ions. Upon oxidation the remote electron transfer occurs between pairs of \{Fe^{II}(Tp)(CN)$_3$\}/\{Fe^{III}(Tp)(CN)$_3$\} through Fe^{II}-CN-Fe^{III}-CN-Fe^{III}. Upon reduction however, the electron transfer passes through the \{Fe^{III}(pzTp)(NC)$_3$\}/\{Fe^{II}(pzTp)(NC)$_3$\} moieties via Fe^{III}-NC-Fe^{II}-CN-Fe^{II}. Therefore, the bands are similar but not identical and disappear once all the iron ions have been reduced or oxidized.

Section S8 Magnetic properties

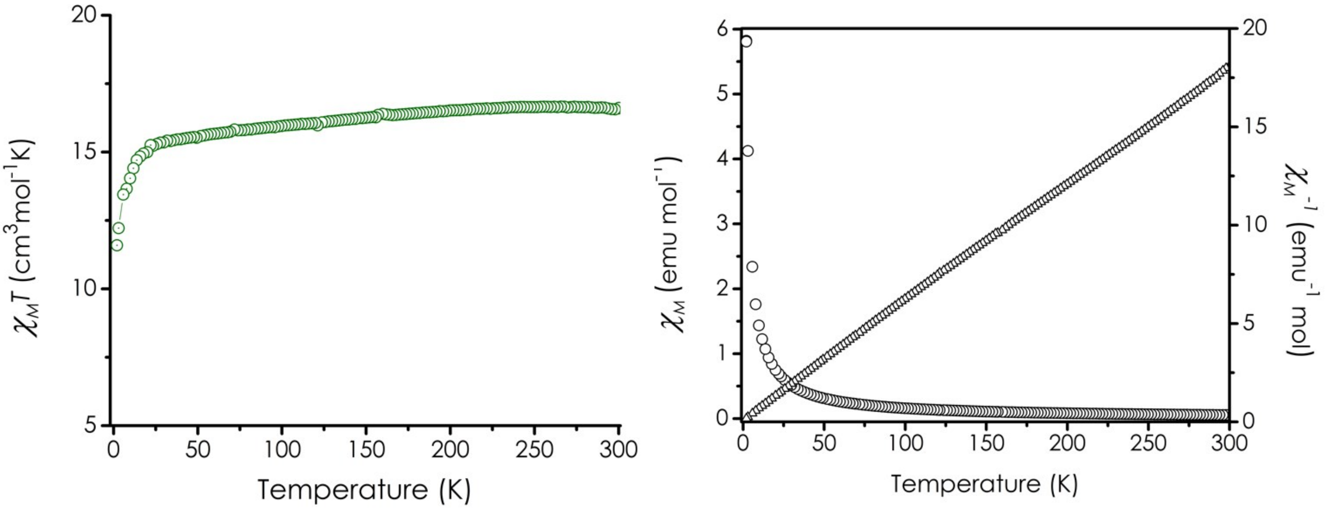

Figure S11. $\chi_M T$ vs. plot (left) and χ_M vs. T plot (right) of a previously dried sample of Cs$\subset$\{Fe$_4$Fe$_4$\}.

Section S9 TGA

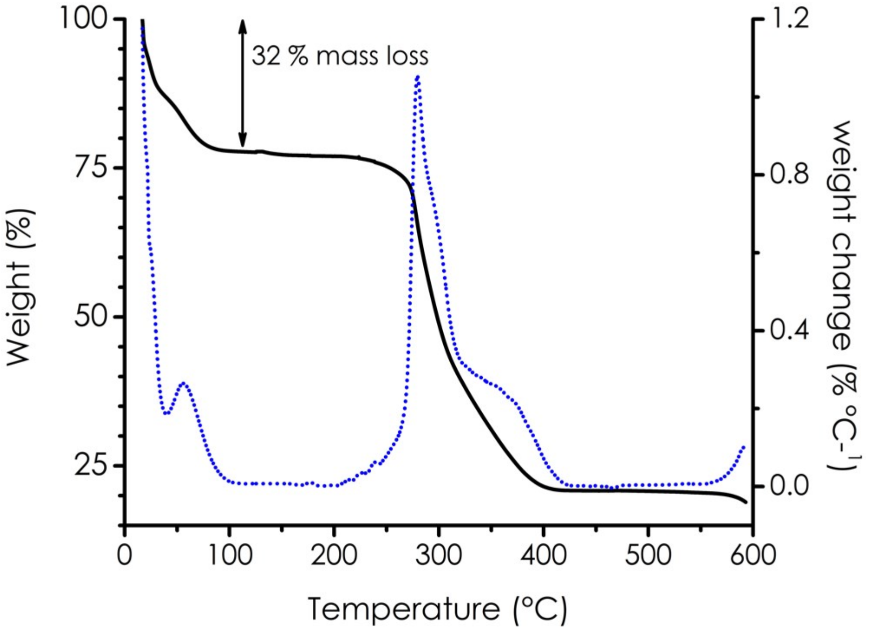

Figure S12. TGA of a freshly prepared sample of Cs⊂{Fe_4Fe_4} in N_2 atmosphere. The black line depicts the weight curve for a given temperature, the dotted blue line the weight change (derivative). The compound rapidly loses solvent molecules (about 32 %) until reaching a plateau at *ca*. 100 K. MW_{sol} = 3315.4 gmol^{-1}

Section S10 Mössbauer spectroscopy

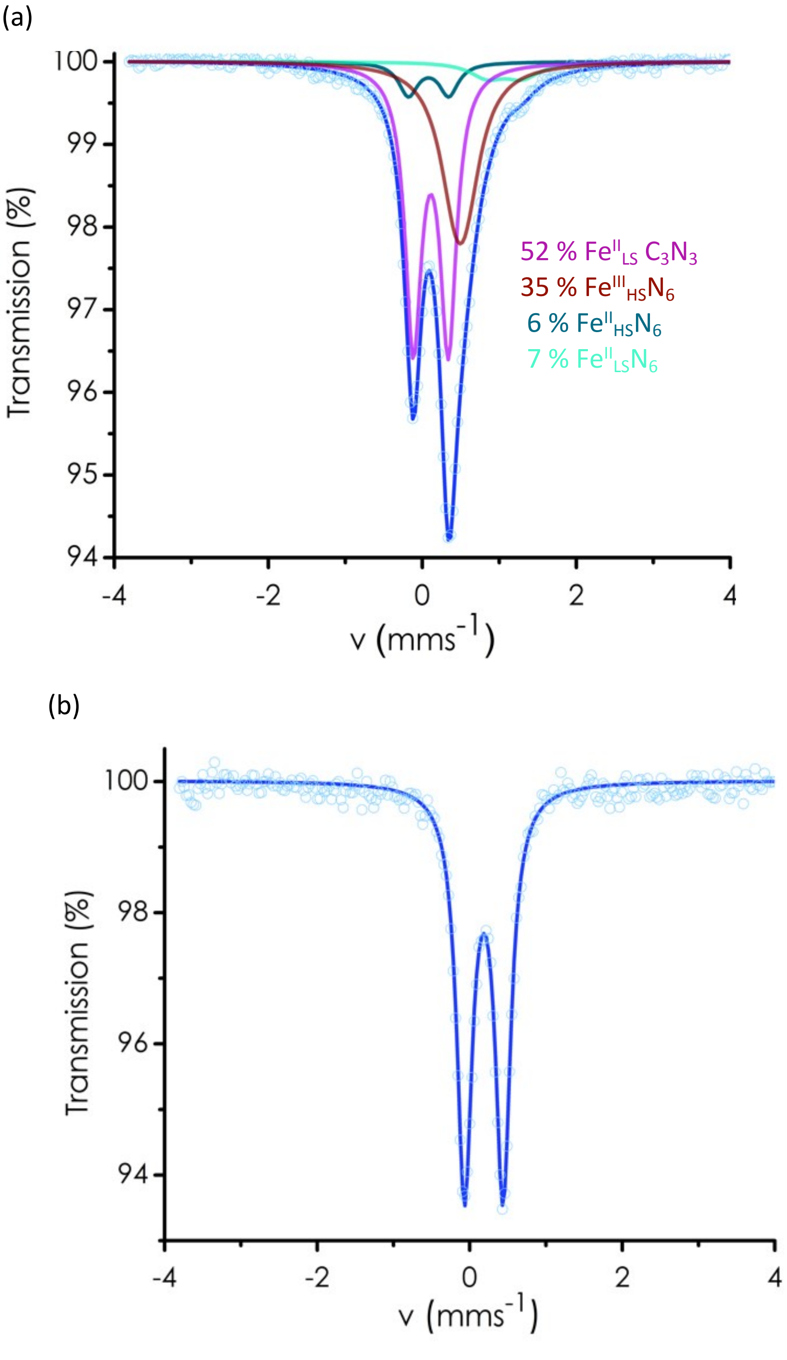

Figure S13. (a) Mössbauer spectra (measured at 80 K) of : (a) a powdered sample of Cs⊂{Fe^{II}_4-$Fe^{III}_3Fe^{II}$}; (b) the analogous Cs⊂{Fe^{II}_4-$Co^{III}_3Co^{II}$} cube showing the contribution of the $Fe^{II}_{LS}C_3N_3$ sites. Experimental data (blue circles); best fit (blue line); $Fe^{II}_{LS}C_3N_3$ (red line); $Fe^{III}_{HS}N_6$ (violet line); $Fe^{II}_{LS}N_6$ (dark cyan line) and $Fe^{II}_{HS}N_6$ (light cyan line).